coatings

MDPI

Article

Investigation on Microstructure and Properties of Cold-Sprayed Ni-Mo-Al_2O_3 Composite Coating

Yinqing Gong [1,†], Cong Xiao [2,†], Shunjie Hu [1], Yicheng Zhou [1], Chenglin Li [1], Bing Yang [1], Jianqiang Zhang [1] and Guodong Zhang [1,*]

1 School of Power and Machinery, Wuhan University, Wuhan 430072, China; gongyinqing@whu.edu.cn (Y.G.); 2020282080098@whu.edu.cn (S.H.); 2022102080012@whu.edu.cn (Y.Z.); lichenglin211@whu.edu.cn (C.L.); toyangbing@whu.edu.cn (B.Y.); zhangjq123456@163.com (J.Z.)
2 School of Mechanical and Electrical Engineering, Wuhan Qingchuan University, Wuhan 430204, China; xcong613@126.com
* Correspondence: guodongzhang_whu@126.com
† These authors contributed equally to this work.

Abstract: In this work, the effect of Mo on the microstructure and properties of Ni-Mo-Al_2O_3 coatings by cold spraying was studied. The microstructure, composition, hardness, wear resistance and chlorine salt corrosion resistance of the coatings were analyzed by a scanning electron microscope, EDS, X-ray diffractometer, 3D profilometer, microhardness tester and friction wear tester. The results show that the coatings have low porosity and a uniform structure. The addition of Mo can improve the hardness, electrical conductivity, wear resistance and chlorine salt corrosion resistance of the coating but reduce the deposition efficiency of the powder. In general, the 80Ni-10Mo-10Al_2O_3 coating has the best comprehensive performance, with a hardness of 270.17 HV, friction coefficient of 0.4171 and corrosion rate of 0.287 $g/m^2 \cdot h$ in molten chloride.

Keywords: Ni-Mo composite coating; cold spray technology; friction and wear performance; chlorine salt corrosion resistance

check for updates

Citation: Gong, Y.; Xiao, C.; Hu, S.; Zhou, Y.; Li, C.; Yang, B.; Zhang, J.; Zhang, G. Investigation on Microstructure and Properties of Cold-Sprayed Ni-Mo-Al_2O_3 Composite Coating. *Coatings* **2024**, *14*, 205. https://doi.org/10.3390/coatings14020205

Academic Editor: Kyong Yop Rhee

Received: 21 November 2023
Revised: 28 January 2024
Accepted: 2 February 2024
Published: 5 February 2024

1. Introduction

Compared with traditional metal additive manufacturing technology, cold spraying, a new type of surface modification technology, can provide low-temperature conditions for printed metal materials. Materials formed by cold spraying have high density and fewer defects than materials formed by other methods. It has the characteristics of low spraying temperature, no phase change, strong adhesion and wide application range, and it is widely used in additive manufacturing, surface repair and surface modification [1–4].

In more and more industrial environments, molten chloride salts are actively or passively appearing, such as in municipal waste incineration, waste liquid recycling from aluminum smelting processes, and concentrated solar power technology [5–7]. With the strong corrosiveness of the molten chloride salt, its corrosion phenomenon often happens in essential equipment such as boilers for storing molten chloride salt, which decreases the service life of the equipment and increases the industrial production cost. Therefore, the corrosion research of chlorinated molten salts has always been a hot topic at home and abroad. Due to its excellent mechanical properties and corrosion resistance, nickel-based alloys are considered important structural materials for concentrating solar power generation [8].

Nickel-based alloys have excellent mechanical properties and are thus widely used in various fields [9,10]. Therefore, the corrosion behavior of nickel-based alloys in molten chloride has been extensively studied in related fields. Liu [11] compared the corrosion resistance of 304 stainless steel and the In625 alloy in molten salt NaCl-$CaCl_2$-$MgCl_2$ at 600 °C and analyzed the corrosion reasons. The corrosion results showed that compared with 304 stainless steel, the Ni-based alloy In625 has better corrosion resistance, and O_2 and H_2O in the air are the key factors for inducing corrosion. Zhao [12] studied the corrosion behavior of 304, 316L, 321 and 310S stainless steel in NaCl-KCl-$MgCl_2$ ternary mixed molten chloride. The results showed that the oxides MoO_3, NiO and TiO_2 were generated on the alloy surface during the corrosion process, which improved the corrosion resistance of 316L, 310S and 321 stainless steel in molten chloride. Chlorine salt produces Cl_2 at high temperatures, which is the main reason why Cl_2 stainless steel is corroded. Ma [13] studied the corrosion of the In625 alloy and 304 stainless steel in NaCl and KCl as well as $CaCl_2$ and $MgCl_2$, respectively, at 900 °C. The results showed that the corrosion of the alloy in $CaCl_2$ and $MgCl_2$ was more serious than that in NaCl and KCl. In addition, In625 showed better corrosion resistance because of the higher content of Ni and Cr in In625. Zhang [14] also found that under the synergistic effect of sodium chloride and steam, the corrosion of a Fe-Cr alloy was greatly accelerated. It is also speculated that sodium chloride can react with oxides and matrix metals, thus destroying the protection of the Cr_2O_3 oxide scale and accelerating the corrosion of chromium.

Ambrosek [15] found that in binary molten salt, the protective effect of Cr in nickel-based alloys was limited. Le [16] found that the existence of two elements, Ni and Mo, made 316L alloy have the best corrosion resistance. Chen [17,18] found that Ni is not easily corroded by NaCl at 750 °C, but the addition of Cr will react with NaCl and water vapor, and its products will, in turn, react with Ni to corrode it. Adding molybdenum to Ni-Cr alloy can stabilize the NiO-$NiCr_2O_4$-Cr_2O_3 oxide scale formed by the alloy under thermal corrosion and improve the thermal corrosion resistance of the material. Although there is some controversy about whether Cr can effectively prevent the corrosion of molten chloride, many studies above show that Ni and Mo can prevent the corrosion of molten chloride to some extent.

In addition to corrosion resistance, long-distance transportation also puts forward higher requirements for the wear resistance of the storage. At present, there is little research on coatings that are both wear-resistant and resistant to molten salt corrosion. As a kind of metal oxide, Al_2O_3 has a high hardness, low density, high melting point and strong corrosion resistance, and it is a common production in the strengthening phase of coating processes. Therefore, Ni-Mo-Al_2O_3 composite coating has good mechanical properties and molten chloride corrosion resistance in theory, which may have great development potential and application prospects.

This article focuses on the fabrication and characterization of Ni-Mo-Al_2O_3 composite coatings with different Mo contents by cold spraying. And the microstructure, composition, hardness, wear resistance and chlorine salt corrosion resistance of the coatings are analyzed and studied in detail.

2. Materials and Experimental Procedure

2.1. Coating Preparation

The base metal of the test was 304 stainless steel, which is widely used in industrial production. The surfacing materials were pure Ni, pure Mo and pure Al_2O_3 powder supplied by (Huayi Alloy Welding Material Ltd., Beijing, China). The purity of all powders was 99.9%, and the average particle size was 30 μm The specific appearance is shown in Figure 1. The chemical composition (wt.%) is shown in Table 1. Samples with 0 wt.%, 10 wt.% and 20 wt.% Mo are denoted as CS1, CS2 and CS3 hereinafter, respectively. The composite coatings were fabricated by cold spraying (LP-TCY-II, Beijing Tian Cheng Yu New Material Technology Co., Ltd., Beijing, China) with compressed argon as the process gas, and the cold spray process schematic is shown in Figure 2. The air pressure was 0.8 MPa, and a gas preheating temperature of 500 °C was used to increase the gas–solid two-phase flow velocity and promote the plastic deformation of the powder particles. The substrate selected was 304 stainless steel ($100 \times 100 \times 5$ mm^3) and it was shot-peened before cold spraying. The distance between the cold spray nozzle and the substrate was 10 mm, and the moving speed was 4 mm/s.

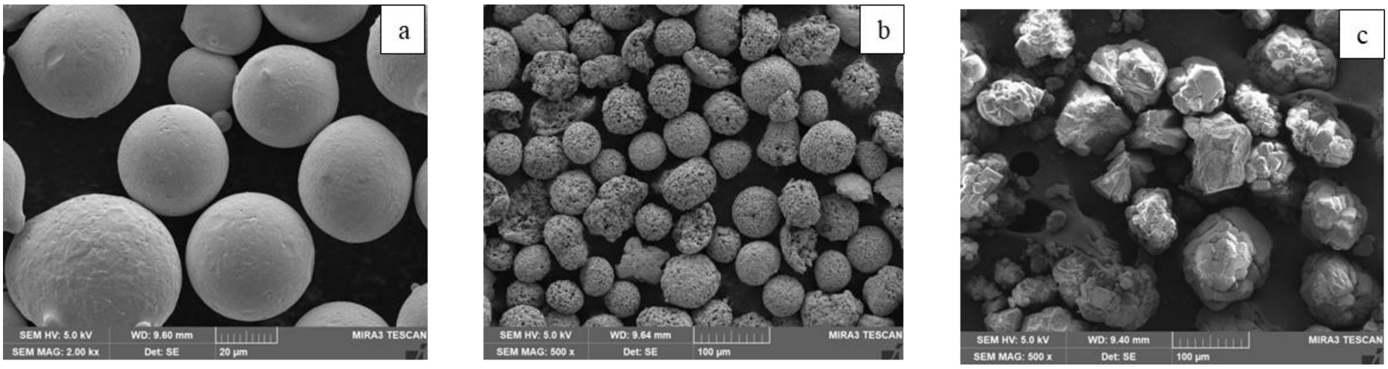

Figure 1. Cold-sprayed powder morphology: (**a**) Ni, (**b**) Mo, (**c**) Al_2O_3.

Table 1. Powder composition of coating material (wt.%).

Sample	Ni	Mo	Al_2O_3
CS1	Bal.	0	10
CS2	Bal.	10	10
CS3	Bal.	20	10

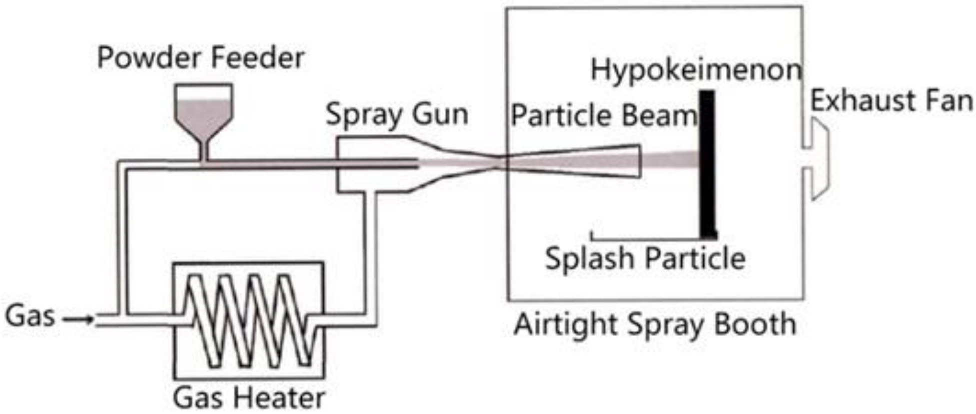

Figure 2. Schematic of the CS additive manufacturing process.

2.2. Coating Characterization

Samples with dimensions of 10 mm × 10 mm × 12 mm were obtained by wire cutting. The samples were ground and polished with metallographic sandpaper and diamond polishing paste. The surface and cross-section morphologies of the three coatings were examined by a 3D profilometer (New View 9000, ZYGO, CT, USA), SEM (MIRA3LMH, Brno, Czech Republic) and EDS. The hardness was measured by a Vickers hardness indenter (HXS-1000A, Shanghai milite Precise Instrument Co., Ltd., Shanghai, China) with a load of 200 g for 10 s. The sample was subjected to a sliding friction test using a ball disc friction tester (MS-T3000, Lanzhou Huahui Instrument Technology Co., Ltd., Lanzhou, China) at room temperature. A 6 mm diameter stainless steel ball was used with a load of 2 N and a speed of 200 r/min. After the friction test, SEM and the 3D profilometer were used to observe the surface of the worn sample.

2.3. Corrosion Resistance Test

Samples with dimensions of 10 mm × 10 mm × 2 mm were obtained by wire cutting the coatings. The composition of molten chloride refers to the composition of molten chloride waste liquid recycled by a titanium smelting process: 50 wt.% NaCl + 33.4 wt.% $MgCl_2$ + 16.6 wt.% $AlCl_3$ in a mass ratio is 3:2:1. The pretreated samples were placed in a corundum crucible containing molten chloride salt and kept in a constant-temperature furnace at 750 °C for 10–20 h until the sample showed obvious corrosion. During this period, the samples were taken out every 1–2 h and weighed with their weight changes recorded every time. The corrosion rate was characterized by the mass change per unit time and unit area of the sample.

3. Results and Discussion

3.1. Microstructure and Composition

Figure 3 shows the microstructure and surface morphology of three different Mo-containing cold-sprayed coatings. As can be seen in Figure 3a–c, Ni, Mo and Al_2O_3 are clearly distinguished from each other, and EDS composition analysis was carried out on three points A, B and C. The results are presented in Table 2. The white flat area is Mo, the black area with sharp edges and corners is Al_2O_3 and the rest is Ni. The three components are evenly distributed. Mo and Al_2O_3 are similar in size, while Ni's distribution seems different. That is because Ni has the characteristics of good plasticity and excellent viscosity, and compared with the other two components, its melting point is lower. During the deposition process, Ni is more prone to severe plastic deformation and adiabatic shear instability. In addition, the excellent viscosity of Ni is also conducive to the deposition of other components on Ni to form a multi-component composite coating based on Ni [19]. As can be seen in Figure 3d–f, the coating has good adhesion with the base material, and the internal composition of the layer is uniform.

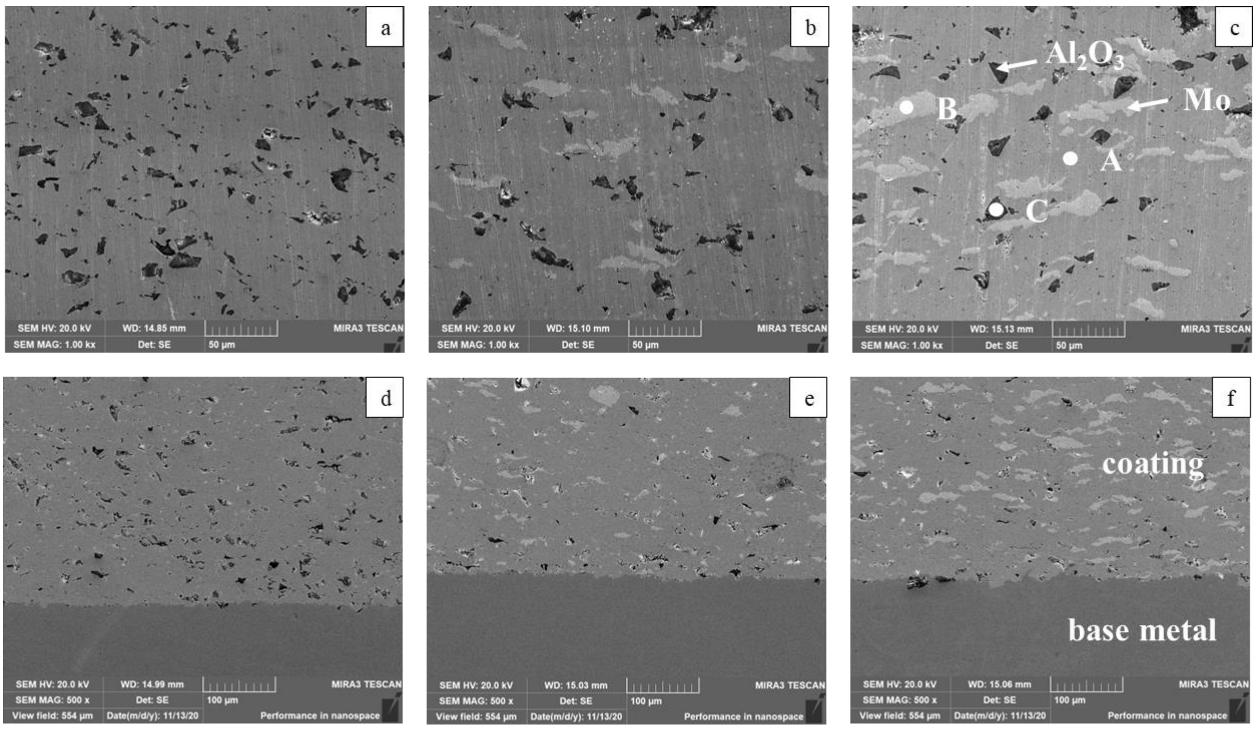

Figure 3. Microstructure and surface profile of cold-sprayed coatings with different Mo contents: (**a**) 0 wt.%, (**b**) 10 wt.%, (**c**) 20 wt.%, (**d**) 20 wt.% (**e**) 10 wt.%, (**f**) 20 wt.%.

Table 2. Chemical composition of cold-sprayed coating with 20 wt.% Mo (wt.%).

Element	Ni	Mo	Al	O
A	98.28	1.12	0.05	0.55
B	1.64	97.59	0.20	0.57
C	2.36	0.67	51.33	45.64

It can be seen from Figure 3 that the microstructure of the three coatings is relatively dense, and the flat Mo particles indicate that the spherical particles have severe plastic deformation. During the deposition of cold-sprayed powder, high-speed particles impact the substrate and produce severe plastic deformation. This drastic change forces dislocations in the grains to intertwine, causing the dislocation density and the number of grain boundaries to increase significantly. As the grains undergo dynamic recrystallization and refinement, a considerable amount of fine Mo particles can be observed [20]. The dynamic recrystallization of powder particles is conducive to improving the microstructure and properties of the coating. The refined grains could extend the binding surface area of the particles, thereby increasing the binding strength, improving the hardness of the coating, increasing the uniformity of the coating microstructure and reducing defects. By virtue of its high hardness and high relative critical velocity, Al_2O_3 has no obvious plastic deformation. However, according to the shape of Al_2O_3 particles, this oxide will be severely broken during high-speed impact, which makes its distribution in the coating more uniform. Particles deposited by cold spraying undergo initial deformation during impact, resulting in their adhesion to previously deposited particles, followed by further deformation due to impact on particles, resulting in compaction. In this case, the Al_2O_3 particles with high hardness deposited on the previous Ni, resulting in greater plastic deformation and increasing the compaction effect. The mechanism elaborated on above explains the low porosity of the coating.

Comparing Figure 3a–c, it is found that the deposition rate of CS3 coating alumina is the lowest; that is to say, it is significantly lower than that of CS1 and CS2, which is on account of the hardness of Mo. The increase in Mo content affects the deposition efficiency of hard-phase Al_2O_3. It can be found in Figure 3c that the three components have obvious plastic deformation and mechanical occlusion, which greatly increase the contact area between different elements, thereby enhancing the bonding force, which is manifested as a decrease in porosity and an increase in hardness. An XRD test of the CS3 cold-sprayed coating was carried out, and the scanning results were analyzed by Jade (version 6) software. As shown in Figure 4, it can be found that the cold-sprayed coating did not lead to metallurgical bonding, and Ni, Mo and Al_2O_3 belonged to mechanical mixing, with their own single-phase regions.

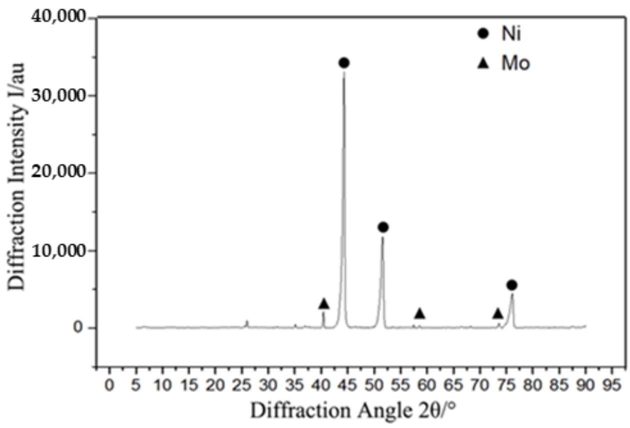

Figure 4. XRD phase of CS3 coating.

3.2. Hardness

During the hardness test, five points are taken from each area at an interval of 0.5 mm along the direction from the base metal to the coatings. Figure 5 shows the cold-sprayed coating microhardness distribution. The microhardness of the coating has a similar behavior, but the microhardness value fluctuates greatly. It may be that the hardness of Al_2O_3 and molybdenum is much greater than that of nickel, while Al_2O_3, Mo and Ni are not metallurgically combined, inducing inhomogeneous microscopic composition; therefore, the composition in the loading area of the microhardness probe significantly affects the test results. The area where the loading area happens to be Al_2O_3 or molybdenum exhibits a higher test hardness, while the area where the loading area is nickel exhibits a lower test hardness. The average hardness of the three coatings is higher than the base 304 stainless steel with a hardness of about 190 HV. Among them, the average hardness of the CS2 coating is the largest, which is due to the high hardness and high melting point of Mo. The addition of 20 wt.% Mo is not conducive to the deposition of alumina, resulting in the lowest Al_2O_3 content of the CS3 coating. The CS2 coating contains a lot of Al_2O_3 and harder Mo, its distribution is the most evenly dispersed, and its compaction effect is the greatest; to sum up, this coating has the greatest hardness.

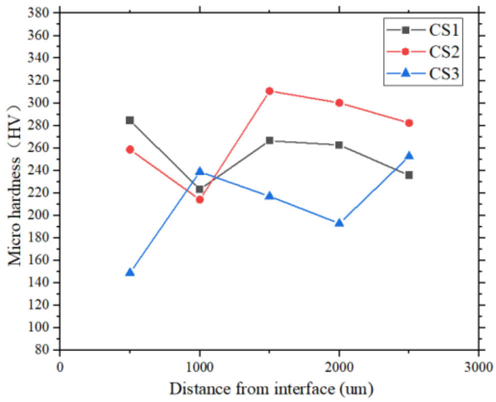

Figure 5. Microhardness distribution of cold-sprayed coatings.

3.3. Friction and Wear Performance

Figure 6 shows the friction curves of three cold-sprayed coatings. It can be seen that the CS2 coating with a Mo content of 10 wt.% has the lowest coefficient of friction, namely 0.4171. At the same time, the volume loss of the CS2 coating is the least among the cold-sprayed samples. Judging from the friction curve, the rising period of CS2 is the shortest, which has the most stable curve and the longest friction coefficient numerical stability zone.

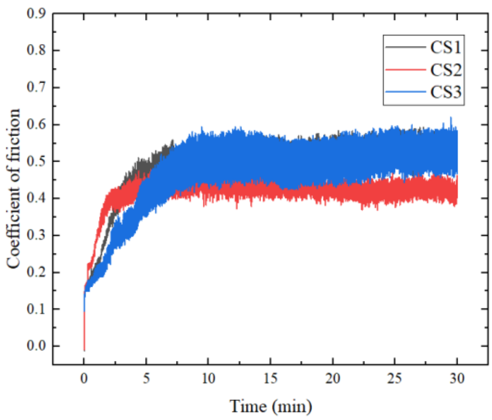

Figure 6. Coefficient of friction of the Ni-Mo-Al_2O_3 composite coatings.

Figure 7 shows the microstructure and surface profile of the cold-sprayed coatings with different Mo contents. As shown in Figure 7a–c, the wear surface morphology of the coatings with different Mo additions at room temperature mainly has defects such as adhesion pits, oxide layers and scratches. The wear mechanism is mainly manifested as adhesive wear. The coating heats up during the friction process, and as the temperature rises, the surface is quickly oxidized by oxygen in the air, and an oxide layer is formed to adhere to the surface of the coating. Since the oxide layer is relatively flat, it can play a role in lubrication when worn and can reduce the friction coefficient. In addition, since most metal oxides have higher hardness than pure metals, they could have an effect of increasing the surface hardness, which can effectively hinder the grinding and extrusion of the grinding ball on the substrate to improve the wear resistance of the sample. It should be noted that the thickness of the oxide layer is limited and relatively brittle. Due to the repeated friction and rolling shear force of the grinding ball, the surface of the oxide layer in contact with the grinding ball will be fatigued and damaged, and part of it will fall off and form adhesion pits. Most of the oxide layer that has fallen off will be crushed by the grinding ball and converted into the form of wear debris, which causes scratches on the worn surface. A small part of the oxide layer that has fallen off will be embedded in the relatively soft matrix after repeated grinding and will play a certain role in wear resistance in the subsequent wear process [21–23].

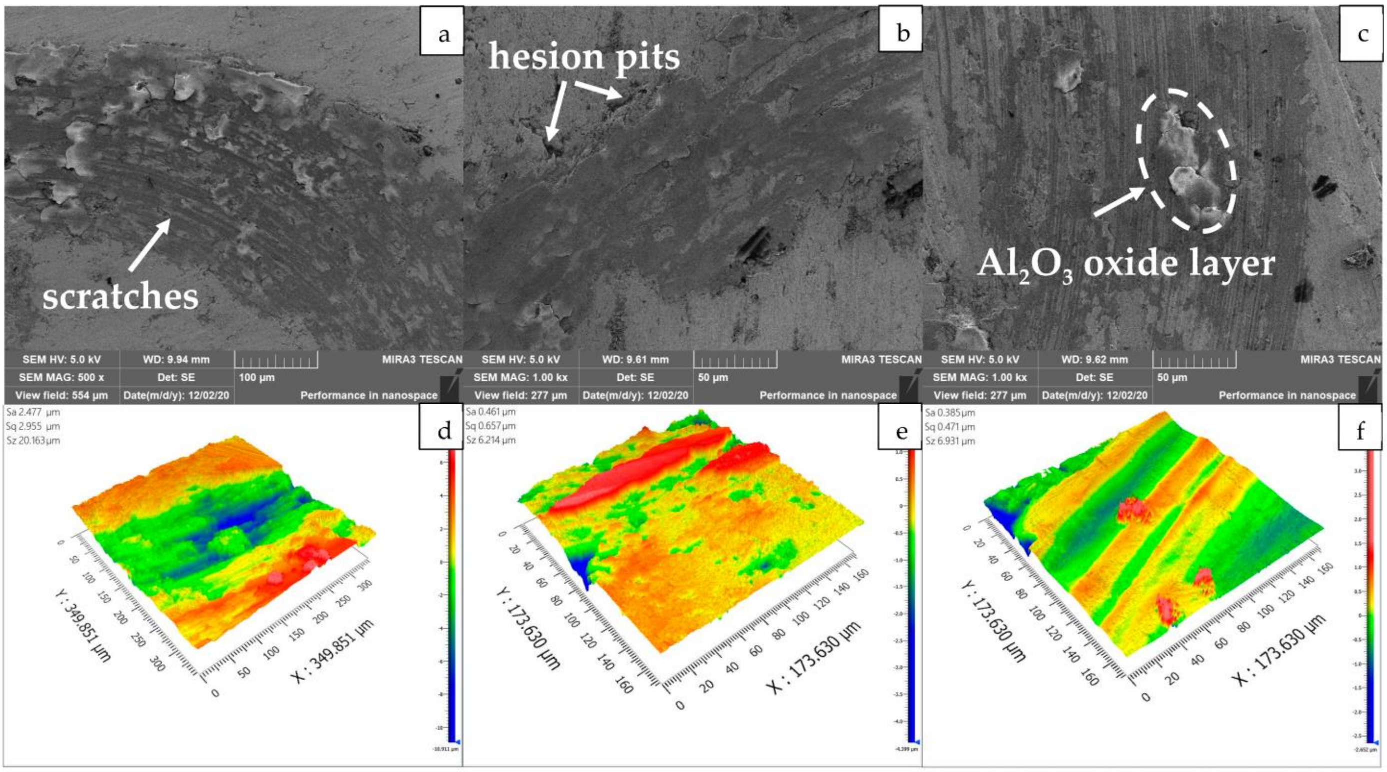

Figure 7. Microstructure and surface profile of the cold-sprayed coating with different Mo contents: (**a**) 0 wt.%, (**b**) 10 wt.%, (**c**) 20 wt.%, (**d**) 0 wt.%, (**e**) 10 wt.% and (**f**) 20 wt.%.

From the wear surface, as shown in Figure 7d–f, the oxide layer of the CS1 coating has a large shedding area. There are many small particles near the wear groove and a great number of scratches in the groove. It indicates that the wear of the CS1 coating includes abrasive wear and adhesive wear [14]. The CS2 coating has protrusions in the grooves, exhibiting that there are components with higher hardness that have not fallen off. The groove of the CS2 coating is relatively flat, the adhesion pit is smaller and shallower and there is no visible small scratch. It shows that the wear of the CS2 coating is mainly adhesive wear, so its quality loss is the smallest and the friction coefficient is the smallest as well, but the wear resistance is the best. Obvious Al_2O_3 particle protrusions can be seen in the CS3 coating. On account of its high hardness, the Al_2O_3 is embedded in the cladding layer in the form of a hard phase. During the friction and wear process, the alumina acts as a buffer and protection part for the other components of the coating. In addition, the outer edge of the CS3 coating groove has the highest bulge and the oxide layer is the thickest. The oxide layer hinders the grinding and extrusion of the grinding ball to the substrate and improves the wear resistance of the CS3 coating. Since there are no small abrasive particles around the groove and no other scratches, it can be inferred that the abrasive particles are less worn, which leads to a relatively small friction coefficient of the CS3 coating.

3.4. Corrosion Resistance Performance

Figure 8 shows the corrosion weight change curve of the cold-sprayed coating in molten chloride salt. It can be seen that the weight of the specimens shows a slight increase in the beginning, then a slight decrease emerges during the corrosion period. In the early stage of corrosion, oxide films such as NiO and MoO_3 are formed on the surface of the coating, which makes the total mass of the coating slightly augmented. As the corrosion progresses, the Cl_2 generated by the reaction passes through the passivation layer on the surface of the coating. Metal oxides react with Cl_2 to generate corresponding metal chlorides. Because the vapor pressure of metal chlorides is low at high temperatures, the metal chlorides diffuse out of the coating under the drive of free energy, leaving pores, making the total mass of the coating decrease slightly [22]. Meanwhile, these pores provide a path for the chlorine gas to enter the deeper coating, so that the oxidation reaction continues until the surface of the passivation layer sample leaves visible holes [24].

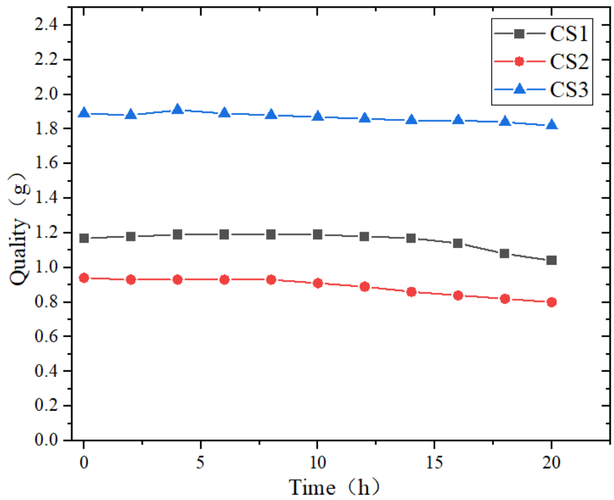

Figure 8. Corrosion weight change curve of cold-sprayed coatings.

Figure 9 shows the microscopic morphology and XRD phase analysis of the cold-sprayed coating after corrosion. It can be seen that obvious corrosion marks appear on the surface of the coating, and the surface becomes uneven and more pores appear. The CS1 coating has more holes and a smaller size, the CS2 coating has fewer holes but more gaps, and the CS3 coating has fewer holes and gaps but a larger size. A partial area of the sample surface is taken for EDS composition analysis, and the results are shown in Table 3. The Ni content of the coating gradually decreases and the Mo content gradually increases, which is consistent with the original content of the coating. There is a large amount of oxygen on the surface, which indicates serious oxidation. The CS2 coating has the lowest O and Cl composition and the highest Mg composition. From the XRD phase analysis after corrosion, it can be seen that the main component of the surface of the CS1 coating is Ni, in addition to a small amount of NiO. The surface of the CS2 coating is mainly composed of Ni, in addition to a small amount of NiO and MoO_3. The surface of the CS3 coating is mainly composed of Ni, in addition to a small amount of NiO, MoO_3 and Al_2O_3, which shows that the surface of the cold-sprayed coating has not been significantly passivated, and only a partial chemical reaction occurs on the surface of the coating to form a dense oxide film.

After the molten chloride salt corrosion, the presence of a small amount of NiO and MoO_3 can be detected, indicating that part of the surface has a protective effect on NiO and MoO_3. The small amount of NiO and MoO_3 indicates that there is no dense passivation layer that completely covers the coating. After corrosion, in the microscopic morphology, the holes inside the materials can be seen in the sample, indicating pitting corrosion. Using HSC Chemistry software (version 8) to perform thermodynamic calculations, it is found that both Ni and Mo can undergo oxidation reactions at 750 °C. Except for the reaction of Mo and O_2, which forms MoO_3, the Gibbs free energy of other oxidation reactions is close to zero. Although those reactions can occur spontaneously at 750 °C, their reaction speed is relatively low. As Mo is oxidized in the first place, Ni oxidizes at a slower rate, and there is no oxidation reaction on the coating surface in a short period of time. Therefore, the corrosion rate of the cold-sprayed coating is much lower than that of the 304 stainless steel substrate.

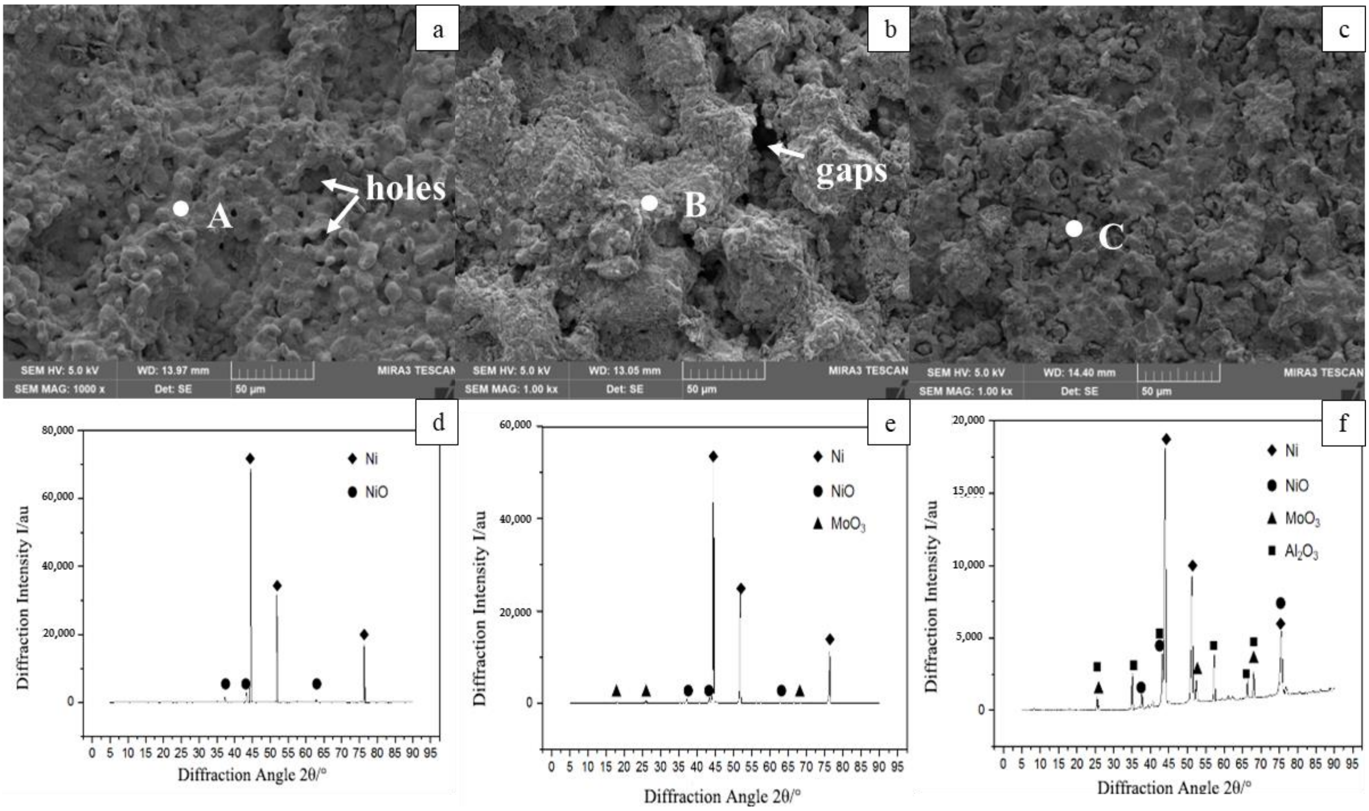

Figure 9. Micro-corrosion morphology and XRD phase of cold-sprayed coatings with different Mo contents: (**a**) 0 wt.%, (**b**) 10 wt.%, (**c**) 20 wt.%, (**d**) 0 wt.%, (**e**) 10 wt.% and (**f**) 20 wt.%.

Table 3. Chemical composition of micro-area after corrosion of cold-sprayed coatings (wt.%).

Element	Ni	Mo	O	Al	Cl	Mg	Na
A	71.05	—	21.19	4.65	3.12	—	—
B	68.79	4.46	16.61	4.03	1.96	3.19	1.05
C	52.81	13.26	27.61	1.32	2.97	2.02	—

4. Conclusions

In view of the fact that existing molten chloride corrosion-resistant coatings cannot give consideration to both corrosion resistance and wear resistance, a new corrosion-resistant coating is proposed in this study, and its actual effect is considerable, but the related in-depth corrosion resistance and wear resistance mechanism still need to be studied. The specific conclusions related to this work are as follows:

(1) The cold-sprayed coating is composed of Ni, Mo and Al_2O_3, and there is no metallurgical bond among the components. From the microscopic morphology, both Ni and Mo exhibit adiabatic shear instability. With the occurrence of obvious plastic deformation, the contact area between the two extends, thereby increasing the bonding force. Due to its poor plasticity, Al_2O_3 is crushed during the deposition process, is distributed evenly inside the coating, and exerts a tamping effect.

(2) Mo and Al_2O_3, due to their high hardness, significantly increase the hardness of the coating. The average hardness of the three coatings (≥245 HV) is higher than that of the base 304 stainless steel (190 HV). The content of Mo affects the deposition rate of alumina. As the content of Mo increases, the overall hardness of the coating increases at first and then decreases. The hardness of the 80Ni-10Mo-10Al_2O_3 coating with a Mo content of 10 wt.% is the largest.

(3) The wear surface morphology of the coatings with different Mo additions at room temperature mainly shows defects such as adhesion pits, oxide layers and scratches, and the wear mechanism is mainly manifested as adhesive wear. The 80Ni-10Mo-10Al_2O_3 coating with a Mo content of 10 wt.% has the smallest friction coefficient and the best wear resistance.

(4) With an increase in Mo content, the corrosion resistance of the coating is improved. On the one hand, Mo and alumina can increase the density of the coating; on the other hand, the corrosion resistance of Mo is better than that of Ni, whereas an increase in Mo can significantly improve the overall coating.

(5) The 80Ni-10Mo-10Al_2O_3 coating has the best resistance to molten chloride corrosion and the best mechanical properties, with a hardness of 270.17 HV, friction coefficient of 0.4171 and corrosion rate of 0.287 $g/m^2{\cdot}h$ in molten chloride.

Author Contributions: Methodology, J.Z.; Formal analysis, Y.Z.; Resources, B.Y.; Data curation, S.H.; Writing—original draft, Y.G.; Writing—review & editing, C.X., C.L. and G.Z.; Supervision, B.Y.; Project administration, C.L. and G.Z.; Funding acquisition, C.X. and G.Z. All authors have read and agreed to the published version of the manuscript.

Funding: This research was funded by the Natural Science Foundation of Hubei Province of China (2022CFB435) and the National Key Research and Development Program of China (2017YFB1103900).

Institutional Review Board Statement: Not applicable.

Informed Consent Statement: Not applicable.

Data Availability Statement: Data are contained within the article.

Conflicts of Interest: The authors declare no conflict of interest.

References

1. Luo, X.-T.; Li, Y.-J.; Li, C.-J. A comparison of cold spray deposition behavior between gas atomized and dendritic porous electrolytic Ni powders under the same spray conditions. *Mater. Lett.* **2016**, *163*, 58–60. [CrossRef]
2. Qiu, X.; Tariq, N.u.H.; Qi, L.; Tang, J.-R.; Cui, X.-Y.; Du, H.; Wang, J.-Q. Effects of Dissimilar Alumina Particulates on Microstructure and Properties of Cold-Sprayed Alumina/A380 Composite Coatings. *Acta Metall. Sin. Engl. Lett.* **2019**, *32*, 1449–1458. [CrossRef]
3. Aghasibeig, M.; Monajatizadeh, H.; Bocher, P.; Dolatabadi, A.; Wuthrich, R.; Moreau, C. Cold spray as a novel method for development of nickel electrode coatings for hydrogen production. *Int. J. Hydrogen Energy* **2016**, *41*, 227–238. [CrossRef]
4. Yuan, J.; Wang, Q.; Liu, X.; Lou, S.; Li, Q.; Wang, Z. Microstructures and high-temperature wear behavior of NiAl/WC-Fe x coatings on carbon steel by plasma cladding. *J. Alloys Compd.* **2020**, *842*, 155850. [CrossRef]
5. Xu, X.; Dehghani, G.; Ning, J.; Li, P. Basic properties of eutectic chloride salts NaCl-KC -$ZnCl_2$ and NaCl-KCl-$MgCl_2$ as HTFs and thermal storage media measured using simultaneous DSC-TGA. *Sol. Energy* **2018**, *162*, 431–441. [CrossRef]
6. Ding, W.; Bonk, A.; Bauer, T. Corrosion behavior of metallic alloys in molten chloride salts for thermal energy storage in concentrated solar power plants: A review. *Front. Chem. Sci. Eng.* **2018**, *12*, 564–576. [CrossRef]
7. Mehos, M.; Jorgenson, J.; Denholm, P.; Turchi, C. An Assessment of the Net Value of CSP Systems Integrated with Thermal Energy Storage. *Energy Procedia* **2015**, *69*, 2060–2071. [CrossRef]
8. Loureiro, T.; Sterling, R.; Testani, C.; Torralba-Calleja, E.; Turchetti, L.; Blanco, M.; Ferriere, A.; Perrotta, F. Next Generation of Concentrated Solar Power Technologies. *Proceedings* **2019**, *20*, 361–371.
9. Sarvghad, M.; Maher, S.D.; Collard, D.; Tassan, M.; Will, G.; Steinberg, T.A. Materials compatibility for the next generation of Concentrated Solar Power plants. *Energy Storage Mater.* **2018**, *14*, 179–198. [CrossRef]
10. Yin, Y. *Theoretical Studies on the Surface Behaviors of Nickel-Based Alloys Under Molten Salts Environment*; University of Chinese Academy of Sciences (Shanghai Institute of Applied Physics, Chinese Academy of Sciences): Shanghai, China, 2019.
11. Liu, B.; Wei, X.; Wang, W.; Song, M.; Ding, J. Corrosion behavior of In625 alloy and 316L stainless steel in NaCl-$CaCl_2$-$MgCl_2$ ternary eutectic molten salt. *CIESC J.* **2017**, *68*, 3202–3210.
12. Zhao, Z.; Wang, Y.; Liu, B.; Wei, G. Experimental Study on Corrosion Characteristics of Ternary Mixed Chloride Salt NaCl-KCl-$MgCl_2$. *Power Gener. Technol.* **2018**, *39*, 561–565.

13. Ma, H.; Zhu, M.; Zhao, Y.; Xia, J. Corrosion Behaviors of Two Kinds of Alloys in Chloride Molten Salts. *Mater. Rev.* **2014**, *28*, 109–113.
14. Zhang, X.; Li, H.; Li, S. Research Progress on Corrosion and Damage of Stainless Steel in High Temperature Molten Salts. *Corros. Sci. Prot. Technol.* **2019**, *31*, 349–354.
15. Ambrosek, J.W. *Molten Chloride Salts for Heat Transfer in Nuclear Systems*; University of Wisconsin-Madison: Madison, WI, USA, 2011.
16. Wang, L.; Li, B.; Shen, M.; Li, S.-Y.; Yu, J.-G. Corrosion resistance of steel materials in LiCl-KCl melts. *Int. J. Min. Met. Mater* **2012**, *19*, 930–933. [CrossRef]
17. Chen, L.Y.; Lan, H.; Huang, C.B.; Yang, B.; Du, L.Z.; Zhang, W.G. Hot corrosion of Ni, Cr, and 80Ni20Cr in the presence of NaCl and water vapor at 750 °C. *Mater. Corros.* **2017**, *68*, 1172–1179. [CrossRef]
18. Chen, L.; Lan, H.; Huang, C.; Yang, B.; Du, L.; Zhang, W. Hot corrosion behavior of porous nickel-based alloys containing molybdenum in the presence of NaCl at 750 degrees C. *Eng. Fail. Anal.* **2017**, *79*, 245–252. [CrossRef]
19. Zhu, L.; Hu, S.; Xu, B.; Zhang, G. Fabrication and characterization of Ni-Coated Graphite/Al–Zn coatings by cold spraying. *Surf. Eng.* **2020**, *36*, 1032–1039. [CrossRef]
20. Rokni, M.R.; Widener, C.A.; Ozdemir, O.C.; Crawford, G.A. Microstructure and mechanical properties of cold sprayed 6061 Al in As-sprayed and heat treated condition. *Surf. Coat. Technol.* **2017**, *309*, 641–650. [CrossRef]
21. Hiratsuka, K.; Muramoto, K. Role of wear particles in severe–mild wear transition. *Wear* **2005**, *259*, 467–476. [CrossRef]
22. da Silva, F.S.; Cinca, N.; Dosta, S.; Cano, G.; Guilemany, J.M.; Benedetti, A.V. Influence of cold gas spray parameters on the corrosion resistance of Al-Al_2O_3 coatings sprayed on carbon steel. *Corros. Eng. Sci. Technol.* **2019**, *54*, 567–574. [CrossRef]
23. Zong, L.; Zhou, J.; Yang, Y.; Wang, M. Effect of Mo on the microstructure and properties of Fe-Cr-Mo-C hardfacing layers. *Weld. Technol.* **2021**, *50*, 15–18+105.
24. Gao, R. *The Behavior of Alloy Oxides in High-Temperature Molten Salts Application Environment*; University of Chinese Academy of Sciences (Shanghai Institute of Applied Physics, Chinese Academy of Sciences): Shanghai, China, 2019.